AXIAL MODELLING AND TESTING OF A PIPE RACK

A.S. Tijsseling & A.E. Vardy
Department of Civil Engineering
University of Dundee
Dundee DD1 4HN
United Kingdom

Abstract

The influence of a pipe rack on the dynamic axial behaviour of a straight pipe is investigated by physical experiment and numerical simulation. The pipe-rack interface is modelled by dry friction, the importance of which can be assessed beforehand. An empirical Coulomb friction coefficient, estimated from rigid-body motion, is used in the prediction of the transient response of the pipe-rack system to impact loads. The forces involved in some of the experiments are very small, causing attention to be drawn to unexpected characteristics of the impact used to stimulate transient response.

The work presented herein is part of a research project on waterhammer-induced pipe vibrations. The objectives are (i) to gain more insight into the performance of supports during fluid transients and (ii) to assess the validity of numerical models of the support behaviour. This knowledge is needed in fully coupled fluid-structure interaction (FSI) analyses of liquid-filled pipe systems.

1. Introduction

Fluid-structure interaction (FSI) is a general term used for physical phenomena where moving interfaces between a fluid and a solid make a simultaneous treatment of fluid and structure necessary when modelling the phenomena. In liquid-filled pipe systems, pressure pulsations in the liquid interact with mechanical vibrations of the pipe walls. Adequate numerical models exist which describe coupled liquid-pipe phenomena in the time domain [Bürmann 1975, 1980; Wilkinson & Curtis 1980; Wiggert et al. 1985, 1987; Lavooij & Tijsseling 1989] and in the frequency domain [Wilkinson 1978; Lesmez 1989; Tentarelli 1990; de Jong 1994]. Tijsseling [1996] gives a survey of time-domain literature.

Pipe supports play a crucial role in the dynamic behaviour of liquid-filled pipe systems. In stiffly supported systems, FSI effects may be ignored, so that conventional waterhammer and pipe stress analyses can be sufficient. In flexible systems, FSI effects can be dominant, so that fully coupled analyses are necessary. The influence of support rigidity on waterhammer pressures and pipe stresses has been investigated numerically by Heinsbroek & Tijsseling [1994].

Except for Bürmann et al. [1987, 1988ab], who conducted impressive field measurements, most investigators of FSI mechanisms have undertaken their physical experiments in specially designed test rigs. They have used supports that were, in effect, entirely rigid, entirely flexible or well-defined linearly elastic, and they have obtained good validation of their theoretical models.

In practice, support conditions are often not well-defined. When analysing practical pipe systems, either simplifying assumptions have to be made, the validity of which can only be guessed at, or support characteristics have to be measured, which can be both expensive and troublesome. The influence of wrong assumptions can be assessed in a numerical sensitivity analysis, but this tends to be a laborious procedure.

The present study is part of a larger research project on the suppression of waterhammer-induced pipe vibrations. It deals with the behaviour of practical, non-ideal, supports, especially *pipe clamps* and *pipe racks*. Relevant questions include: Under what circumstances and for what type of vibrations may a support be regarded as rigid? When may a support be neglected entirely? How should the 'elasticity' of supports be measured? What is the influence of the structure to which the support is anchored? What kind of damping mechanisms are involved? This paper is a first attempt to answer some of these questions. The dynamic behaviour of pipe racks is studied, both experimentally and numerically.

A *pipe clamp* holds the entire circumference of a pipe and, typically, connects it via a bar to a floor, wall or ceiling. A *pipe rack* is an even simpler means of support: pipes lying on a rack are prevented from moving vertically downwards, but not upwards. When transient events lift them from their supports due to vertical motion, heavy bouncing may result, thereby generating new transients. The assessment of such behaviour, which demands an accurate representation of anchor motion, is not covered herein.

Lateral movement in the rack's horizontal plane is resisted by friction and is usually limited by constraints. Axial movement is restricted only by friction forces. It is the influence of these forces on coupled axial-stress and pressure wave propagation in liquid-filled pipes that is the focus of the present paper. The aim is to assess when such forces might have a significant influence on overall behaviour - on resonance and noise-related phenomena for example.

2. Laboratory tests

2.1. *Experimental apparatus*

Vardy and Fan's [1989] experimental apparatus (Figure 1) has been adapted to enable the influence of pipe supports to be examined. The main feature of the apparatus is its simplicity. A steel pipe (4.5 m long, 52 mm bore) is suspended by wires and closed at both ends, such that it can be filled with pressurised water. Pipe vibrations are generated by the external impact of a 5 m long solid steel rod. With this apparatus, excellent results have been presented for both longitudinal and flexural vibrations of water-filled pipes [Fan 1989; Vardy & Fan 1989], for tests with cavitation [Fan & Tijsseling 1992; Tijsseling 1993] and for tests with multi-pipe systems [Fan & Vardy 1994; Tijsseling et al. 1994].

By suspending their pipe on two long, thin steel wires so that it can move freely in a nearly horizontal plane, Vardy and Fan [1989] avoided any complications due to supports. In the present investigation this complication is deliberately introduced. An extra support is located close to the middle of the pipe.

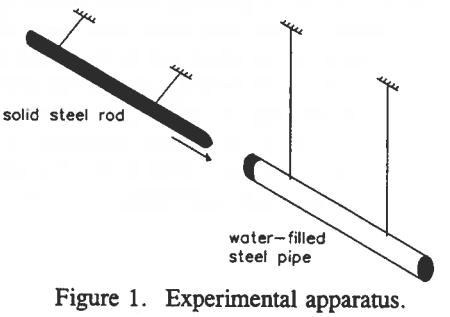

Figure 1. Experimental apparatus.

Pipe vibrations are sensed by strain gauges and by a laser-Doppler vibrometer; liquid pulsations are detected by piezoelectric pressure transducers. Force transducers record the static loads in the suspension wires. Two data acquisition systems allow multi-channel sampling rates up to 125 kHz and 1 MHz respectively. Detailed descriptions of the instrumentation and the measurement procedures are given by Fan [1989] and Tijsseling [1993].

Table 1 lists the data used in the numerical simulations. From these data, the masses of the empty and the water-filled pipe are calculated as 26.6 kg and 36.2 kg respectively. The corresponding measured values are 26.5 kg and 36.3 kg. The total mass (1.6 kg) of the end caps is about 6% of the empty pipe's mass. The mass of the rod is calculated as 79.4 kg.

Steel pipe	Water
L_t = 4502 mm R_t = 26.01 mm e = 3.945 mm E_t = 168 GPa ρ_t = 7985 kg/m^3 ν = 0.29 m_1 = 1.312 kg m_2 = 0.3258 kg	K = 2.14 GPa ρ_f = 999 kg/m^3
	Solid steel rod
	L_r = 5006 mm R_r = 25.37 mm E_r = 200 GPa ρ_r = 7848 kg/m^3

Table 1. Input data for simulations.

2.2. *Pipe rack*

The influence of a pipe rack is simulated in the apparatus by a heavy, solid, steel cylinder transverse to the pipe, near to its midlength (Figure 2). By slightly changing the length of the suspension wires, the weight resting on the supporting cylinder can be varied from zero to full. With three supports for one pipe, however, lining out of the system is a time-consuming matter of trial and error.

A range of tests with empty and water-filled pipes has been performed, using rod impact velocities of about 0.110 and 0.012 m/s. To obtain these velocities, the initial horizontal distances between the rod and pipe were 20.2 and 2.6 mm respectively. The rod was hand-released. With 2.0 mm as a practical limit, the smallest reproducible impact possible in the present apparatus is with a velocity of about 0.010 m/s (the largest is with 1.2 m/s). With 0.012 m/s impact, strain gauge measurements were not possible because the noise/signal ratio was too high.

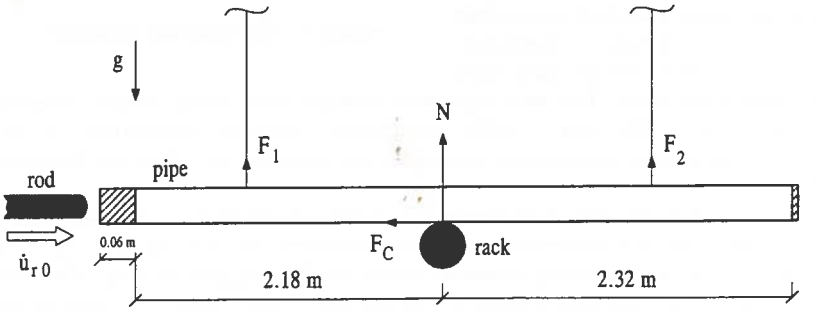

Figure 2. Schematic diagram of pipe-rack configuration.

3. Numerical simulations

3.1. *MOC*

The axial motion of liquid-filled pipes is governed by one-dimensional wave equations which can most conveniently be solved by the method of characteristics (MOC) [Bürmann 1975; Wiggert et al. 1985; Vardy & Fan 1989]. The method traces pressure waves in the liquid and axial-stress waves in the pipe walls and allows for dynamic interaction (FSI) between them. The implementation used herein is fully described by Tijsseling [1993] except for the representation of the pipe support. Flexural and torsional pipe motion are not simulated herein.

3.2. *Wave propagation speeds*

The wave propagation speeds in the experimental apparatus (based on data in Table 1) are, according to the classical (uncoupled) waterhammer and beam theories,

$$c_r = \left(\frac{E_r}{\rho_r}\right)^{\frac{1}{2}} = 5048.2 \text{ m/s} \tag{1}$$

$$c_t = \left(\frac{E_t}{\rho_t}\right)^{\frac{1}{2}} = 4586.9 \text{ m/s} \tag{2}$$

$$c_f = \left(\frac{K}{\rho_f}\right)^{\frac{1}{2}} \left(1 + \frac{2R_t K}{eE_t}\right)^{-\frac{1}{2}} = 1362.5 \text{ m/s} \tag{3}$$

In the case of a water-filled pipe, more correct (coupled) waterhammer and beam theories [Tijsseling 1993] predict 0.7% larger and 0.7% smaller values of c_t and c_f respectively. The deviations from classical theory are quite small in the relatively *thick*-walled *water*-filled *steel* pipe studied herein. In the case of an 'empty' pipe, equation (3) is discarded - that is, the influence of contained air (at atmospheric pressure) is neglected.

3.3. *Rod*

The compatibility equations for axial-stress wave propagation in the rod are

$$\frac{\mathrm{d}\sigma_r}{\mathrm{d}t} \mp \rho_r c_r \frac{\mathrm{d}\dot{u}_r}{\mathrm{d}t} = 0 \tag{4}$$

3.4. *Pipe*

The compatibility equations used herein for coupled axial-stress and pressure wave propagation in a liquid-filled pipe are those given by Tijsseling & Lavooij [1989]. For the present study, they do not differ greatly from the following simplified forms which

are much easier to understand:

Pipe
$$\frac{d\sigma_t}{dt} \mp \rho_t c_t \frac{d\dot{u}_t}{dt} + \nu \frac{R_t}{e} \{ (\frac{c_t}{c_f})^2 - 1 \}^{-1} \{ \frac{dP}{dt} \pm \rho_f c_t \frac{dV}{dt} \} = 0 \qquad (5)$$

Liquid
$$\frac{dP}{dt} \pm \rho_f c_f \frac{dV}{dt} - 2\nu \frac{\rho_f}{\rho_t} \{ (\frac{c_t}{c_f})^2 - 1 \}^{-1} \{ \frac{d\sigma_t}{dt} \mp \rho_t c_f \frac{d\dot{u}_t}{dt} \} = 0 \qquad (6)$$

In this model, the axial strain ε_t is equal to $\{ \sigma_t - \nu (R_t/e) P \} / E_t$.

The equations for an empty (i.e. air-filled) pipe are obtained by ignoring equation (6) and by setting $\nu = 0$ in equation (5).

3.5. *Boundary conditions*

3.5.1. Rod-pipe impact

The following four equations are used to model the instantaneous axial rod-pipe impact:

$$\dot{u}_r = \dot{u}_t \qquad (7)$$
$$\sigma_r = 0 \qquad (8)$$
$$\dot{u}_t = V \qquad (9)$$
$$A_r \sigma_r = A_t \sigma_t - A_f P - m_1 \ddot{u}_t \qquad (10)$$

Contact:	Eqs. (7), (9) and (10) are junction conditions for rod and pipe
Separated:	Eqs. (8), (9) and (10) are boundary conditions for rod and pipe
Separation:	occurs when the assumption of contact leads to $\sigma_r > 0$ (tensile)
Multiple impact:	occurs when the assumption of separated conditions leads to $u_r > u_t$

The junction conditions for an empty pipe are obtained by ignoring equation (9) and by setting $P = 0$ in equation (10).

3.5.2. Remote end of pipe

The boundary conditions at the remote end of the pipe are equation (9) and

$$A_t \sigma_t + m_2 \ddot{u}_t = A_f P \qquad (11)$$

In the case of an empty pipe, equation (9) is discarded and $P = 0$ in equation (11).

3.5.3. Remote end of rod

The boundary condition for the remote end of the rod is equation (8).

3.5.4. Pipe rack

Dry friction between a rack and a vibrating pipe is taken into account in the axial junction condition

$$\{A_t \sigma_t\}_1 + F_C = \{A_t \sigma_t\}_2 \tag{12}$$

where the indices 1 and 2 indicate the pipe at the left and right sides of the rack, respectively. The Coulomb friction force

$$F_C = f_C N \operatorname{sign}(\dot{u}_t) \tag{13}$$

acts opposite to the direction of motion of the pipe (Figure 2). The Coulomb friction coefficient f_C and the normal force N on the pipe are assumed to be constant. The assumed sign of $\dot{u}_t$ is compared in each time step with the newly predicted value of $\dot{u}_t$, and adjusted if necessary. When, at some time step, the contradicting situation occurs that with a positive F_C a negative $\dot{u}_t$ is calculated and with a negative F_C a positive $\dot{u}_t$, the friction force F_C is taken equal to zero.

The friction force (13) makes the system non-linear, because (i) it is independent of the impact velocity $\dot{u}_{r0}$ and (ii) the sign($\dot{u}_t$) function is discontinuous.

3.6. *Numerical grid*

A fixed-grid MOC approach is used to simulate the series: free end, rod, multiple-impact interface, pipe, rack, pipe, closed free end. The rod and the two pipe reaches (fluid + solid) are divided into elements having a common computational time step Δt. A fine computational grid is used for the pipe, both spatially and temporally, so that the rack is located exactly at a grid point. A spatially-coarse, but temporally-fine, grid is used for the rod. Interpolations are avoided by employing spatially refined grids and slightly changed wave speeds (not more than 1%). The properties of the computational grids are listed in Table 2, where Δt is taken 5 times smaller than strictly necessary to keep the adjustments in wave speeds small. Details of the numerical implementation are given in [Tijsseling 1993].

Pipe-rack simulations											
Δt (μs)	N_r	N_{t1}	N_{t2}	Δz_r (m)	Δz_{t1} (m)	Δz_{t2} (m)	c_r (m/s)	$c_{t1} = c_{t2}$ (m/s)	$c_{f1} = c_{f2}$ (m/s)	c_t/c_f	i_{OUT}
4.34/5	2	109	116	2.50	0.02	0.02	5050.2	4608.3	1355.4	17/5	50
No-axial-support simulations											
Δt (μs)	N_r	N_{t1}	N_{t2}	Δz_r (m)	Δz_{t1} (m)	Δz_{t2} (m)	c_r (m/s)	$c_{t1} = c_{t2}$ (m/s)	$c_{f1} = c_{f2}$ (m/s)	c_t/c_f	i_{OUT}
54.1/5	2	9	9	2.50	0.25	0.25	5025.1	4617.5	1358.1	17/5	5

Table 2. Properties of numerical grids.

4. Results

Experimental and numerical results are given first for the pipe hanging on its long suspension wires only (Section 4.1) and then for the pipe supported on a rack (Section 4.2).

4.1. *Pipe without supporting rack*

4.1.1. Empty pipe

The impact of the rod (Figure 2) generates a compressive ($\sigma_t > 0$) axial-stress wave travelling towards the remote end of the empty pipe. After about 1 ms ($\approx L_t / c_t$), the compressive wave reaches this free end and reflects as a tensile wave, leaving behind a nearly stress-free pipe. After about 2 ms, the tensile wave reaches the impact end and separates the pipe from the rod. In theory, the whole pipe should then be stress-free and be moving with a constant velocity $\dot{u}_{t0}$, which can be obtained from

$$\dot{u}_{t0} = \frac{2\,m_r}{m_r + m_t}\,\dot{u}_{r0} \tag{14}$$

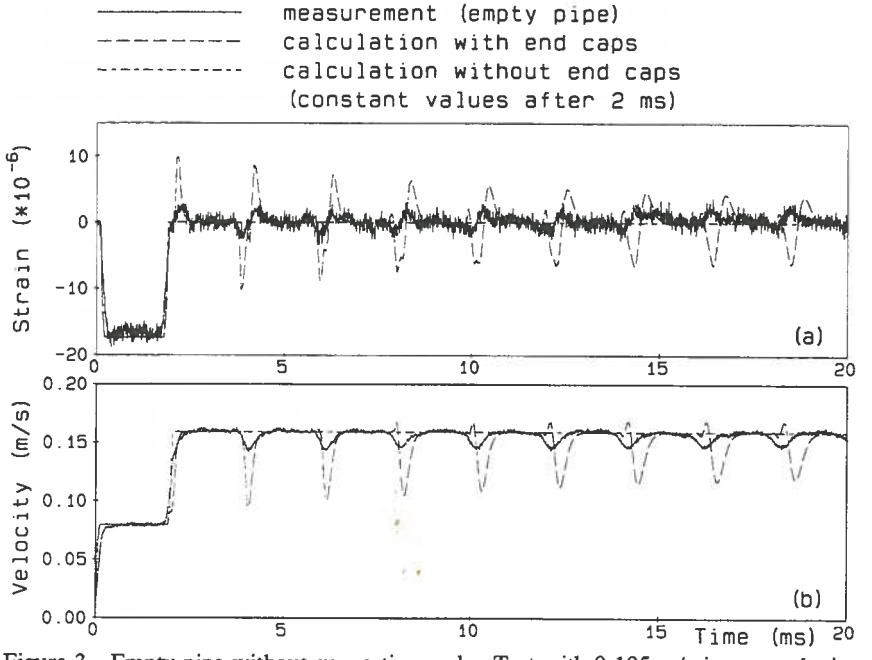

Figure 3. Empty pipe without supporting rack. Test with 0.105 m/s impact velocity: (a) axial strain 574 mm from impact end, (b) axial velocity 46.5 mm from impact end.

a formula valid for the elastic collision of two bodies, if residual vibrations do not occur, which is roughly the case in the present empty apparatus where $2L_r / c_r \approx 2L_t / c_t$. In Figure 3, the rod impact velocity $\dot{u}_{r0}$ input to the simulation is 0.105 m/s, so that the free moving $\dot{u}_{t0}$ should be 0.157 m/s.

Figure 3 shows that the ideal conditions are very nearly reproduced in practice. The axial strain is large during the 2 ms of contact between the rod and the pipe and is nearly constant thereafter. The axial velocity is about 0.08 m/s during contact and about 0.16 m/s thereafter. The real system does not reproduce the ideal behaviour exactly because the pipe is not uniformly elastic. The end caps are mass concentrations that cause the system to vibrate at a frequency of approximately $c_t / (2L_t)$. Indeed, all wave reflections at the pipe ends lead to an elongation of the wave front so that the durations of the periodic dips in the measured velocity signal increase with time.

Two predicted curves are shown in Figure 3. One neglects the end masses and the other treats them as discrete masses at the ends of the pipe. Neither of these representations is exact, but they serve to demonstrate that the periodic dips in the measured velocity are attributable to the end caps. Also, independent simulations (not shown) have indicated that the effect is influenced by the finite rise time apparent in the measured data. A more accurate result can be obtained by modelling the end caps as (very) short elastic rods [Vardy & Fan 1989], but this refinement is not justified for the

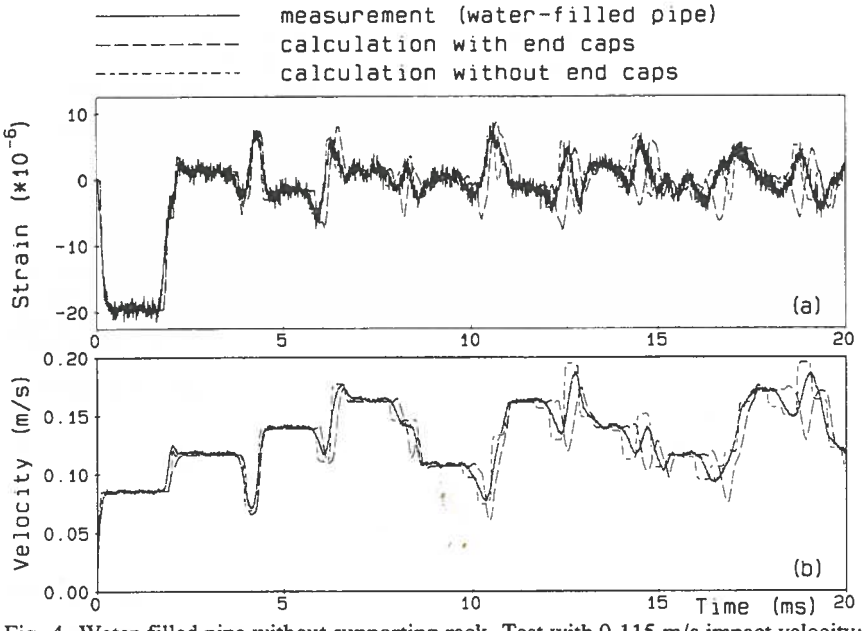

Fig. 4. Water-filled pipe without supporting rack. Test with 0.115 m/s impact velocity: (a) axial strain 574 mm from impact end, (b) axial velocity 46.5 mm from impact end.

purposes of the present study - because the influence of the end caps is much smaller in the case of a water-filled pipe.

4.1.2. Water-filled pipe

A very different result is obtained when the pipe is filled with water (Figure 4) because pressure waves in the liquid have a strong influence. Much better agreement is found between experiment and calculation [Vardy & Fan 1989]. The reproducibility of these experiments is also excellent [Fan 1989]. The influence of the end caps is smaller than in the empty pipe because pressure forces dominate the pipe excitation (equation (11)).

4.2. *Pipe with supporting rack*

4.2.1. Estimation of friction coefficient

The dry friction force F_C acting on a pipe moving on its support is given by equation (13). In general, the normal force N can be estimated from the system's weight and rough values for the friction coefficient f_C can be found in handbooks. In the present case, however, these values have been determined experimentally.

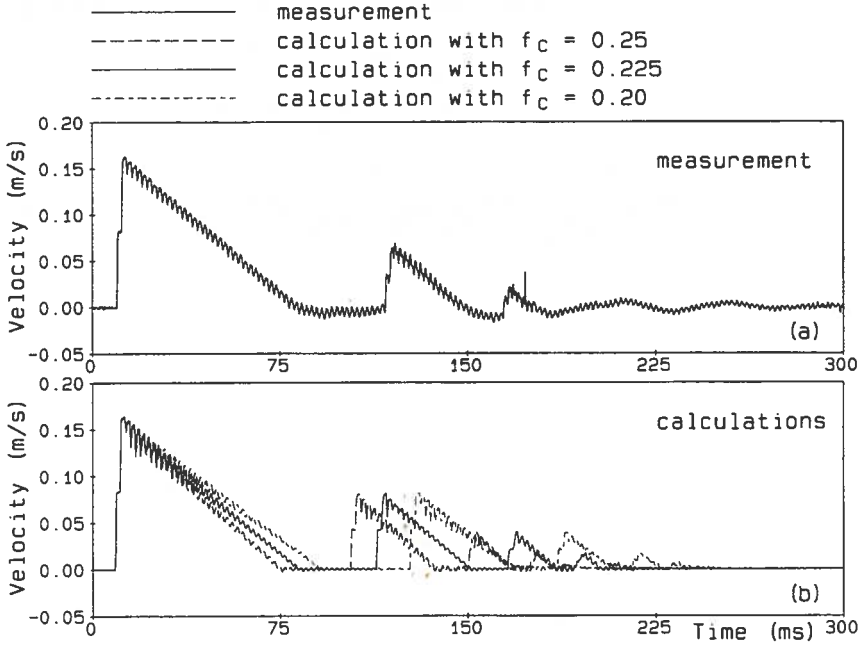

Figure 5. Empty pipe sliding test with 0.110 m/s impact velocity. Pipe velocity close to impact end: (a) measurement, (b) calculations with different friction coefficients.

The normal force on the support is the pipe weight minus the forces in the suspension wires (Figure 2). These forces are nearly constant during any particular experiment. The friction coefficient is obtained from tests with an empty pipe sliding on the support. As explained in subsection 4.1.1, the rod impact gives the unsupported empty pipe an almost constant velocity $\dot{u}_{t0}$ (equation (14)); this is initially true even when the pipe rests on the support, provided that the friction force is small in comparison with the inertia forces. When the support is absent, gravity is the back-driving force and, given sufficient time, the pipe behaves like a pendulum. With the support present, friction is the dominant force and the pipe has a nearly constant deceleration a_0. The friction coefficient is then given by

$$f_C = \frac{m_t a_0}{N} \tag{15}$$

Note that f_C equals a_0/g when the full pipe weight is resting on the support.

Suppose, as a first approximation, that there is a constant deceleration from $\dot{u}_{t0}$ to zero velocity. In this case, the acceleration can be estimated from the measured distance of sliding on the support, s_0, through

$$a_0 = \frac{\dot{u}_{t0}^2}{2 s_0} \tag{16}$$

Strictly, the existence of multiple impacts invalidates the use of this method to estimate f_C. Nevertheless, when the first impact is the largest one, a reasonable estimate of f_C is found. Consider, for example, the test shown in Figure 5a, for which $\dot{u}_{r0} \approx 0.110$ m/s and $N = 24.6 * 9.81 = 241$ N. The total distance s_0 of sliding (measured with a vernier slide gauge) was 6.6 mm and so equations (14), (16) and (15) yield $\dot{u}_{t0} \approx 0.165$ m/s, $a_0 \approx 2.06$ m/s^2 and $f_C \approx 0.23$.

The friction coefficient can alternatively be deduced from the measured velocity history. Figure 5a, obtained with the laser-Doppler vibrometer, shows three clear rod-pipe impacts, each time giving the pipe a new velocity $\dot{u}_{t0}$. The subsequent decelerations are constant, except for the high-frequency vibrations caused mainly by the end caps (see subsection 4.1.1). Small negative velocities are observed, possibly due to flexibility in the solid steel cylinder and/or its mountings.

The regions of above-zero velocity in Figure 5a can be approximated by three triangles with bases and heights 69.6 ms * 0.159 m/s, 29.0 ms * 0.065 m/s and 10.1 ms * 0.020 m/s. The slopes following the three impacts indicate accelerations a_0 of approximately 2.28 m/s, 2.24 m/s and 1.98 m/s, respectively. Equation (15) gives the corresponding friction coefficients as 0.25, 0.25 and 0.22. The total area of the three triangles, 6.5 mm, is the approximate distance of sliding, which is consistent with the direct measurement.

A more accurate assessment of the friction coefficient might be obtained from a sensitivity analysis (tuning) as in Figure 5b, where the simulation with $f_C = 0.225$ shows closer agreement with the measurement in Figure 5a. However, the reproducibility of the tests is not ideal (see Figure 6a), although the first impact is nearly reproducible. Small differences in the distance moved following the first impact

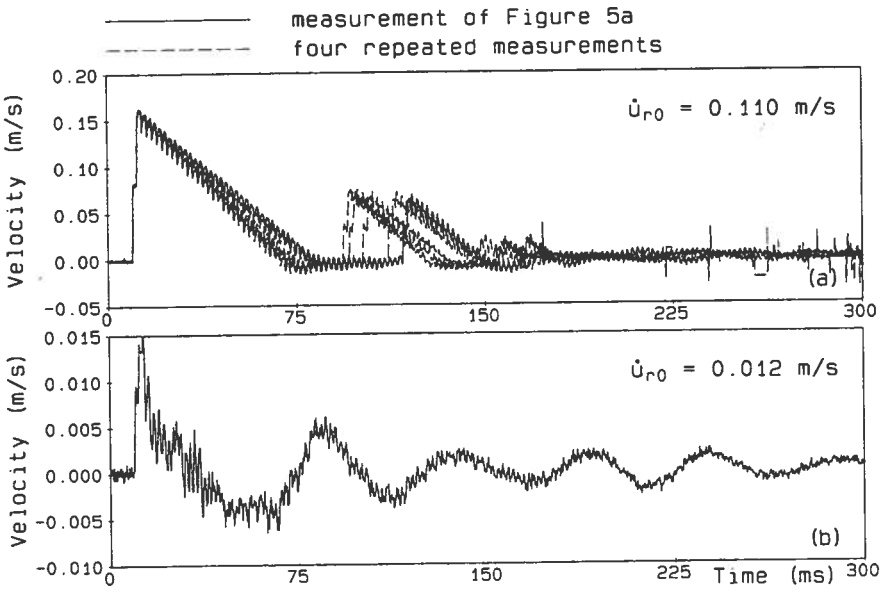

Figure 6. Empty pipe sliding tests. Pipe velocity close to impact end:
(a) reproducibility of tests with 0.110 m/s impact velocity.
(b) test with 0.012 m/s impact velocity.

have a big influence on the timing of subsequent impacts. Also, tests with a very low impact velocity, about 0.012 m/s, exhibit a different behaviour (see Figure 6b). The total sliding distance is negligible in this case (0.1 mm or less) and pipe vibration, rather than rigid-body motion, is the dominant phenomenon. After the transient phase (first 20 ms after impact), the pipe is oscillating on the support with a frequency of about 20 Hz determined by the mass of the pipe and the elasticity of the support.

4.2.2. Importance of dry friction force

In practice, dry friction between a rack and a pipe will usually be much smaller than other forces in typical FSI applications. When the normal force N in equation (13) is due solely to the weight of the pipe and its contents, the force F_C will be much smaller than dynamic forces such as $A_t \sigma_t$ during the most important periods. Nevertheless, it will influence damping during the later stages of large-FSI incidents and it could have a large influence in small-FSI cases. For pipes which are firmly clamped to the rack, the friction forces can be significantly larger.

A quantitative guideline can be inferred from equation (12), namely that friction forces F_C may be neglected if

$$F_C << A_t \sigma_t \tag{17}$$

The dynamic forces $A_t\,\sigma_t$ in typical waterhammer applications are of the order of $A_f \Delta P$, where $A_f \Delta P$ is the unbalanced axial force acting on an unrestrained pipe reach of length L. With Joukowsky's formula, $\Delta P = \rho_f c_f \Delta V$, and considering pressure rise times relative to L / c_f [Uffer 1993], it will usually be easy to estimate the relative magnitudes of the two terms in equation (17).

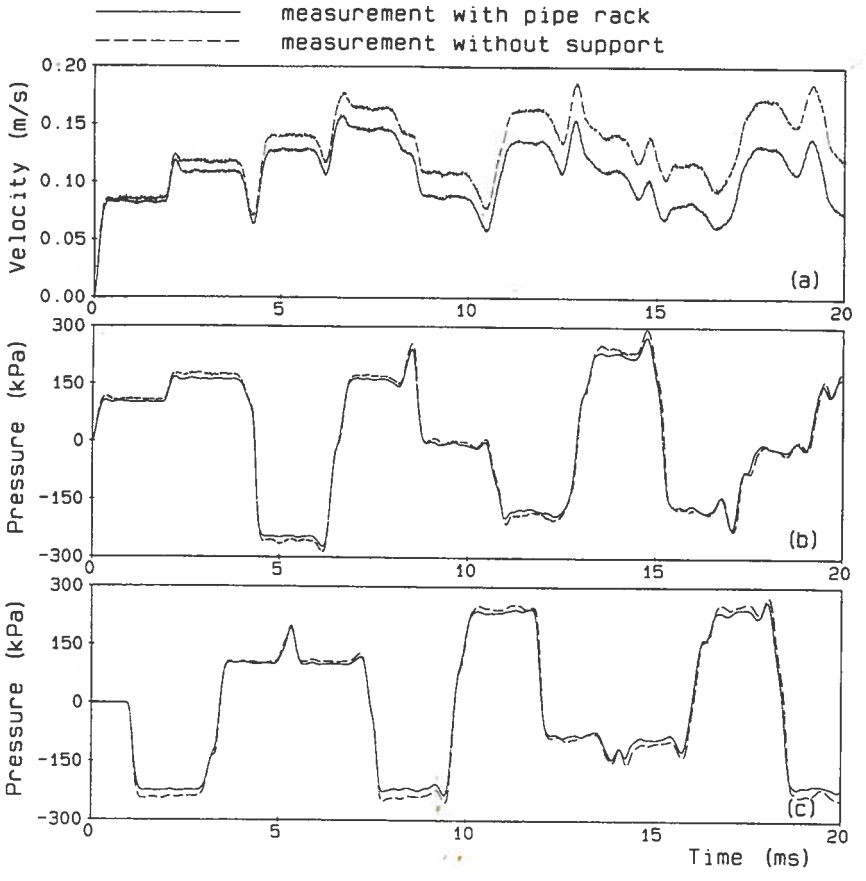

Figure 7. Water-filled pipe. Tests with 0.110 m/s impact velocity:
(a) axial pipe velocity 46.5 mm from impact end,
(b) dynamic pressure 19.5 mm from impact end,
(c) dynamic pressure at remote end.

4.2.3. Water-filled pipe

Water-filled pipe tests have been performed (i) with a rod impact velocity $\dot{u}_{r0} \approx 0.110$ m/s and 15%-20% of the pipe's dead weight resting on the support, (ii) with $\dot{u}_{r0} \approx 0.110$ m/s and 95%-99% dead weight, and (iii) with $\dot{u}_{r0} \approx 0.012$ m/s and 99% dead weight. The measured sliding distances in the three cases were 20-30 mm, 6-7 mm and ≤ 0.1 mm respectively. The reproducibility of the transient phase of all tests was good.

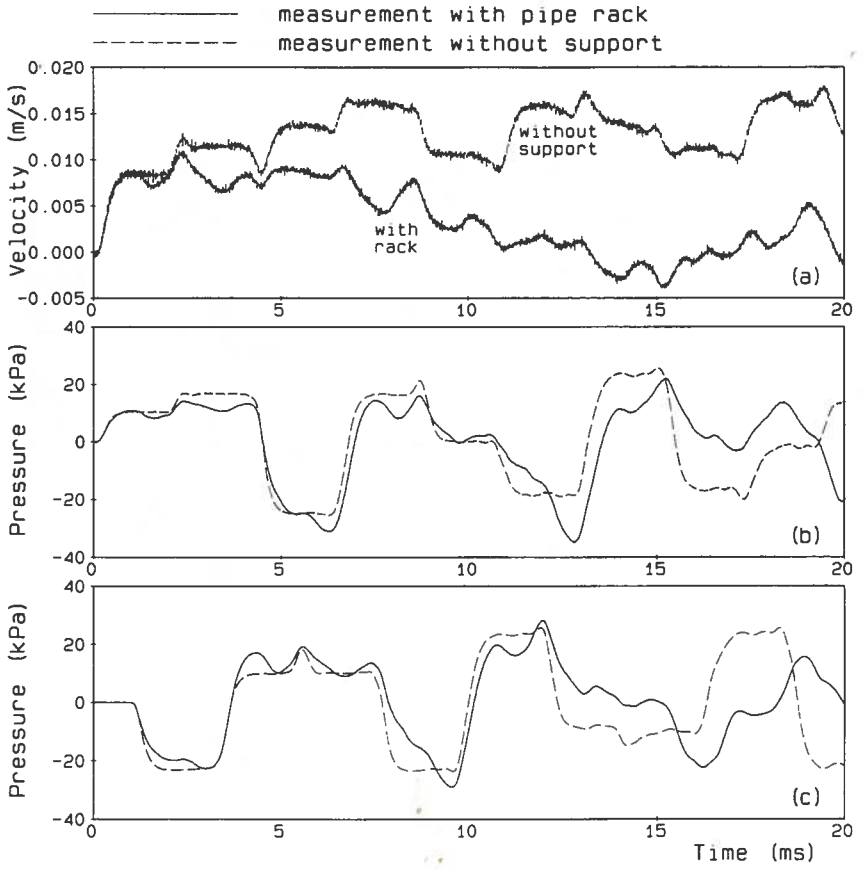

Figure 8. Water-filled pipe. Tests with 0.012 m/s impact velocity:
(a) axial pipe velocity 46.5 mm from impact end,
(b) dynamic pressure 19.5 mm from impact end,
(c) dynamic pressure at remote end.

The friction force is considerable when the full weight of the pipe is resting on the rack (cases ii and iii); to give an indication, it is difficult to make the pipe slide by simply pushing it by hand. Nevertheless, its influence on the system's transient response (first 20 ms) is not significant when the impact velocity is about 0.110 m/s, as shown in Figure 7. That is, the friction force F_C is much smaller than the forces associated with the principal stress waves. A greater influence is exhibited in Figure 8 for the

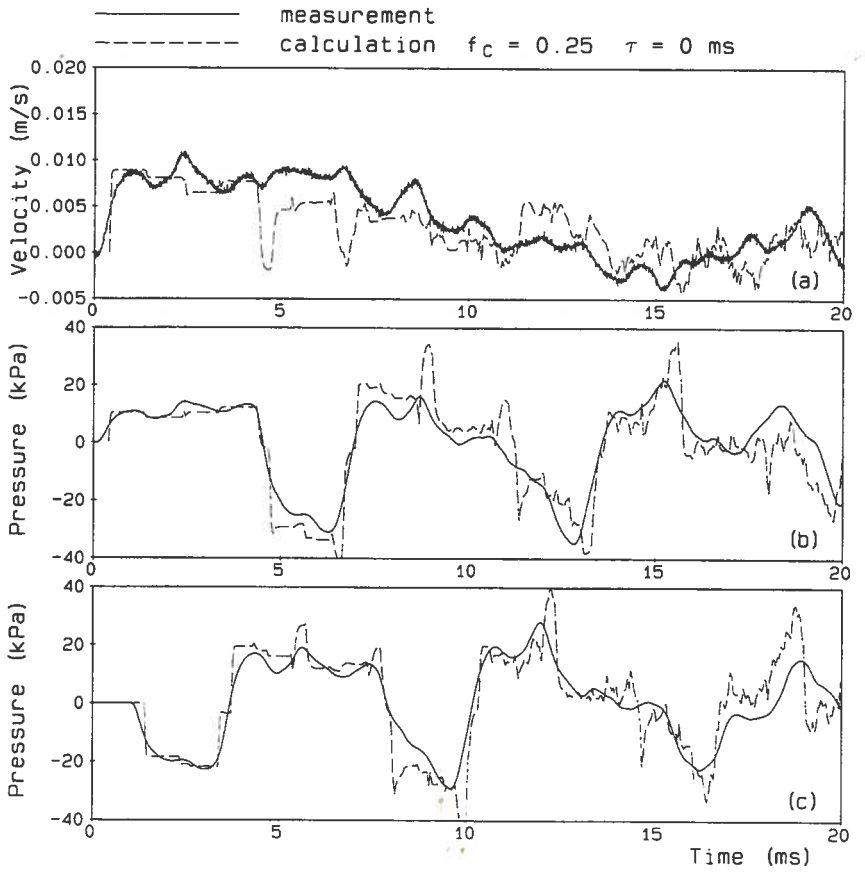

Figure 9. Water-filled pipe with supporting rack. Test with 0.012 m/s impact velocity:
(a) axial pipe velocity 46.5 mm from impact end,
(b) dynamic pressure 19.5 mm from impact end,
(c) dynamic pressure at remote end.

smaller impact velocity of 0.012 m/s. (Note that larger extreme pressures occur in the supported pipe.) In this case, the friction force (approximately a quarter of the total weight of the pipe and water) is not negligible.

To quantify guideline (17): the maximum axial forces $A_f P$ ($\approx A_t \sigma_t$) acting on the closed pipe ends are approximately $2.13 * 10^{-3} * 270 * 10^3 = 575$ N for case (ii), and $2.13 * 10^{-3} * 30 * 10^3 = 64$ N for case (iii). These values, estimated from the Figures 7b,c & 8b,c and compared with the friction force $F_C = f_C m_t g = 0.25 * 36 * 9.81 = 88$ N, confirm condition (17).

The measured results for case (iii) are compared with numerical predictions (with $f_C = 0.25$) in Figure 9. The theoretical predictions are less smooth than the measured results (see next paragraph), but the agreement is otherwise quite good. Consider, for example, the velocity history (Figure 9a). The predicted curve reproduces the trend of the experimental curve, which itself is very different from the corresponding curve with no rack (Figure 8a). Similarly, the predicted pressure histories reproduce the trends of the measured 'with rack' curves much more closely than the 'without support' curves (Figures 8b,c & 9b,c), the differences being most clear in the period after about 10 ms.

The greater smoothness of the measured pressure histories in comparison with the theoretical predictions merits discussion because it is attributable to an interesting effect - albeit one that has no direct relationship to the principal purpose of this paper.

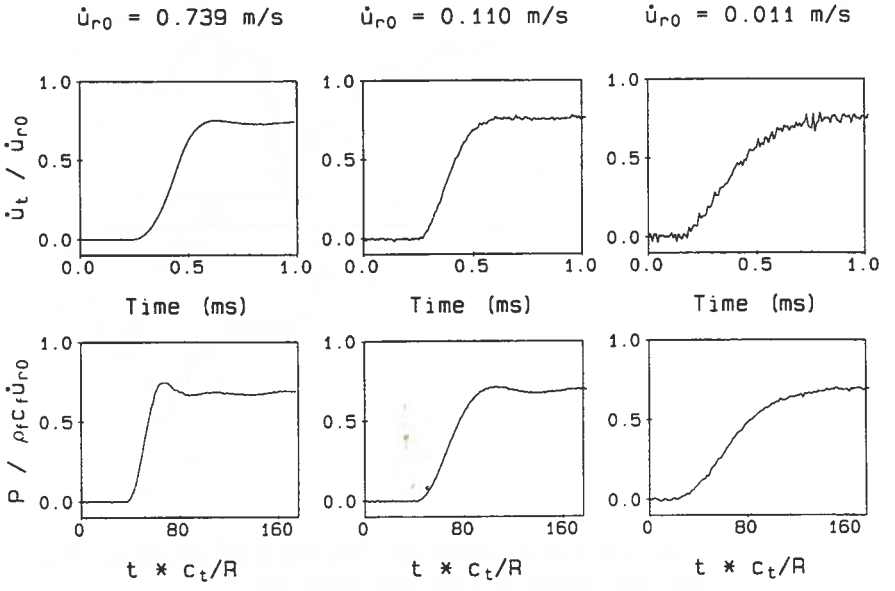

Figure 10. Measured rise times of dimensionless axial velocity and pressure for three different impact velocities. Both dimensionless and dimensional timescales are shown.

The cause is illustrated in Figure 10, which shows the first transient induced by impact of the rod. By inspection, the rise time of this event is much larger with small impacts than with larger ones. This non-linear phenomenon, observed also by Becker & Conway [1964], is probably due to local effects close to the rod's impact point, but the precise mechanism has not been pursued.

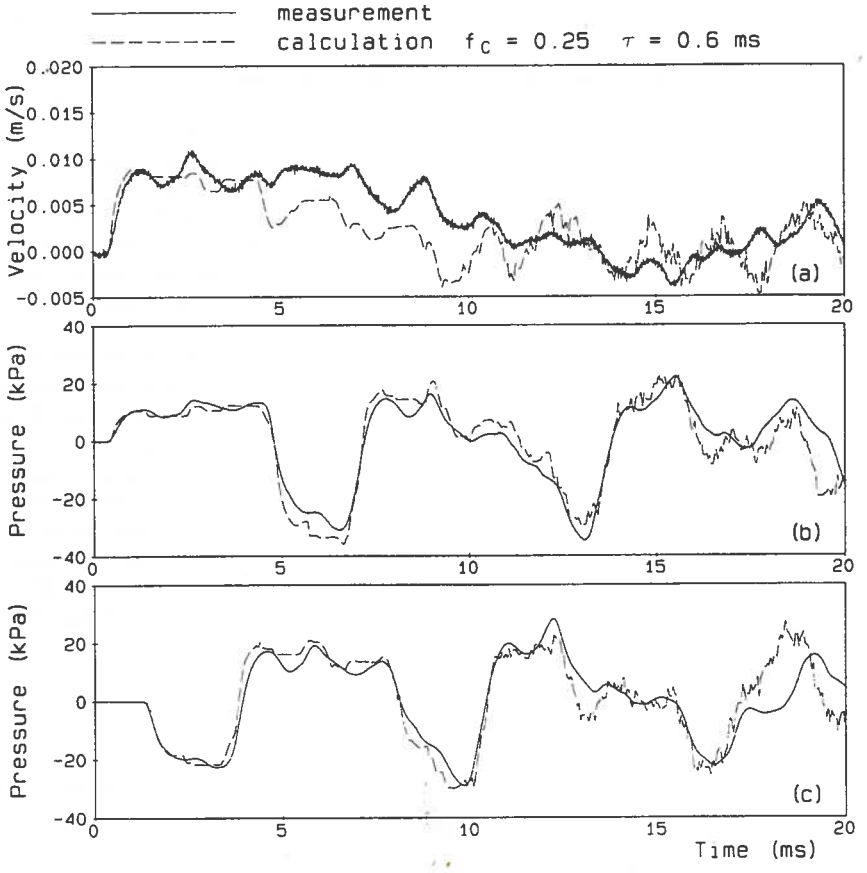

Figure 11. Water-filled pipe with supporting rack. Test with 0.012 m/s impact velocity, calculation with finite rise time of 0.6 ms:
(a) axial pipe velocity 46.5 mm from impact end,
(b) dynamic pressure 19.5 mm from impact end,
(c) dynamic pressure at remote end.

For present purposes, the principal importance of this experimental behaviour is that it detracts from the inherent simplicity of the overall apparatus. It invalidates the implicit assumption in the theoretical model that the impact may be regarded as instantaneous. That is, phenomena that are assumed to occur within one time increment (however small this may be) should instead be simulated as more gradual events. This has not been done in Figure 9 and, as a consequence, the predicted curves are much more erratic than the measured ones.

Long wave fronts lead to an overall smearing effect. In the measured data of Figure 9, the minimum length of a stress wave front is the rise time τ multiplied with the wave speed c_t, that is 0.6 ms * 4587 m/s = 2.75 m, which is long compared to the pipe length. The pressure waves, which travel 3.4 times slower than the stress waves, have 0.8 m long fronts. In the calculated data of Figure 9, the rise time is Δt and the length of a stress wave front is Δz (see Section 3.6), so that wave fronts are steeper in finer numerical grids. As a consequence, in the fine grid used here, smearing does not occur. On the contrary, steep waves (spikes) are generated in increasing numbers by the reflections of pressure and stress waves at the pipe ends and rack. They are also caused by (i) lumped end masses used in a fine numerical grid (see subsection 4.1.1), (ii) multiple rod-pipe impact and separation, and (iii) the dry friction force acting as an impact load when it changes sign (equation (13)). Once generated, the spikes persist since physical and numerical damping are absent.

A second and a third rod-pipe impact were predicted in the 20 ms shown in Figure 9. With calculated separation distances less than 10 μm, a mismatch between experimental and theoretical multiple-impact is inevitable. Fortunately, however, these have little influence on the predicted conditions in the low-impact case.

The results of a simulation with one single, but non-instantaneous, rod-pipe impact are shown in Figure 11. The impact force exerted by the rod is modelled as increasing linearly from zero to its maximum value, $\rho_r c_r A_r(\dot{u}_t - \dot{u}_{r0})$, within a time interval τ = 0.6 ms. Important is that the rod-pipe separation is also modelled gradually: the contact force decreases linearly until it becomes tensile and separation is a fact. As might be expected, the correspondence between measurement and computation is much better now.

5. Conclusions

1. A series of experiments has enabled the influence of axial friction between a pipe and a simple support rack to be assessed with reasonable accuracy. The experiments have provided measurements of pressures and velocities induced by axial impact of the pipe by a long steel rod. In cases with sufficiently high impact, axial strains have also been measured.
2. The measurements have been interpreted directly and by comparison with theoretical predictions based on a fully-coupled FSI analysis previously presented by Tijsseling [1993]. The analysis has been extended by a representation of axial restraint using

a Coulomb friction coefficient. Good quantitative agreement has been demonstrated in large-impact cases and good qualitative agreement has been found in all cases.

3. The cases studied range from those where support friction has little influence (high-impact) to those where it has a pronounced influence (low-impact).
4. A simple, quantitative guideline - equation (17) - has been proposed to enable the likely influence of axial support friction to be assessed at the outset of a design.
5. An unexpected by-product of the work has been the identification of non-linear influences on the rise-time of impacts between the rod and the pipe. It is not sufficient to regard very gentle impacts as effectively instantaneous. With the smallest impacts used herein, the rise time is approximately 0.6 ms.

Acknowledgements

This work is part of a research project on the *Suppression of waterhammer-induced vibrations* sponsored by the EPSRC (Grant GR/J 54857) and guided by an FSI Advisory Group consisting of Keith Austin (Flowmaster), David Clucas (Flowguard), David Fan (JP Kenny), Anton Heinsbroek (Delft Hydraulics), Simon Pugh (ESDU) and Douglas Warne (EPSRC). Ernie Kuperus and Colin Stark have assisted extensively in the design, construction and execution of the laboratory experiments.

References

Becker E.C.H. & Conway H.D. 1964 *Generation and use of mechanical step transients in dynamic measurement.* British Journal of Applied Physics, Vol. 15, pp. 1225-1231.

Bürmann W. 1975 *Water hammer in coaxial pipe systems.* ASCE Journal of the Hydraulics Division, Vol. 101, No. HY6, pp. 699-715. (Errata in Vol. 101, No. HY12, p. 1554)

Bürmann W. 1980 *Längsbewegung frei verlegter Rohrleitungen durch Druckstöße.* (Longitudinal motion of pipelines laid in the open due to water hammer.) 3R international, Vol. 19, No. 1/2, pp. 84-91 (in German).

Bürmann W., Feser G., Janson H. & Thielen H. 1987 *Druck- und Beschleunigungsmessungen an der Rohrbrücke einer Fernwasserleitung zur Untersuchung der Rohrleitungsdynamik bei instationärer Durchströmung.* (Pressure and acceleration measurements on the pipe bridge of a long-distance water main to study the piping dynamics in case of unsteady flow.) 3R international, Vol. 26, No. 9, pp. 638-646 (in German).

Bürmann W. & Thielen H. 1988a *Untersuchung der Bewegung des Befüllstrangs einer Salzkaverne.* (Study on the motion of the filling string of a saline cavern.) 3R international, Vol. 27, No. 4, pp. 275-281 (in German).

Bürmann W. & Thielen H. 1988b *Messung und Berechnung der dynamischen Auflagerkräfte durchströmter Rohre.* (Measurement and computation of dynamic reactive forces on pipes containing flow.) 3R international, Vol. 27, No. 6, pp. 434-440 (in German).

Fan D. 1989 *Fluid-structure interactions in internal flows.* Ph.D. Thesis, The University of Dundee, Dep. of Civil Engineering, Dundee, UK.

Fan D. & Tijsseling A. 1992 *Fluid-structure interaction with cavitation in transient pipe flows.* ASME Journal of Fluids Engineering, Vol. 114, No. 2, pp. 268-274.

Fan D. & Vardy A.E. 1994 *Waterhammer including fluid-structure interactions*. Proc. of the First Int. Conf. on Flow Interaction, Hong Kong, September 1994, pp. 439-442.

Heinsbroek A.G.T.J. & Tijsseling A.S. 1994 *The influence of support rigidity on waterhammer pressures and pipe stresses*. Proc. of the Second Int. Conf. on Water Pipeline Systems, BHR Group, Edinburgh, Scotland, May 1994, pp. 17-30; London, UK: Mechanical Engineering Publications, ISBN 0-85298-921-0.

Jong C.A.F. de 1994 *Analysis of pulsations and vibrations in fluid-filled pipe systems*. Ph.D. Thesis, Eindhoven University of Technology, Eindhoven, The Netherlands, ISBN 90-386-0074-7.

Lavooij C.S.W. & Tijsseling A.S. 1989 *Fluid-structure interaction in compliant piping systems*. Proc. of the 6th Int. Conf. on Pressure Surges, BHRA, Cambridge, UK, October 1989, pp. 85-100.

Lesmez M.W. 1989 *Modal analysis of vibrations in liquid-filled piping systems*. Ph.D. Thesis, Michigan State University, Dep. of Civil and Environmental Engineering, East Lansing, USA.

Tentarelli S.C. 1990 *Propagation of noise and vibration in complex hydraulic tubing systems*. Ph.D. Thesis, Lehigh University, Dep. of Mechanical Engineering, Bethlehem, USA.

Tijsseling A.S. & Lavooij C.S.W. 1989 *Fluid-structure interaction and column separation in a straight elastic pipe*. Proc. of the 6th Int. Conf. on Pressure Surges, BHRA, Cambridge, UK, October 1989, pp. 27-41.

Tijsseling A.S. 1993 *Fluid-structure interaction in case of waterhammer with cavitation*. Ph.D. Thesis, Delft University of Technology, Faculty of Civil Engineering, Communications on Hydraulic and Geotechnical Engineering, Report No. 93-6, ISSN 0169-6548, Delft, The Netherlands.

Tijsseling A.S., Fan D. & Vardy A. 1994 *Transient fluid-structure interaction and cavitation in a single-elbow pipe system*. Proc. of the First Int. Conf. on Flow Interaction, Hong Kong, September 1994, pp. 346-349.

Tijsseling A.S. 1996 *Fluid-structure interaction in liquid-filled pipe systems: a review*. Journal of Fluids and Structures, Vol. 10, No. 2 (in press).

Uffer R.A. 1993 *Water hammer conservatisms*. ASME - PVP, Vol. 253, Fluid-structure interaction, transient thermal-hydraulics, and structural mechanics, pp. 179-184.

Vardy A.E. & Fan D. 1989 *Flexural waves in a closed tube*. Proc. of the 6th Int. Conf. on Pressure Surges, BHRA, Cambridge, UK, October 1989, pp. 43-57.

Wiggert D.C., Otwell R.S. & Hatfield F.J. 1985 *The effect of elbow restraint on pressure transients*. ASME Journal of Fluids Engineering, Vol. 107, No. 3, pp. 402-406.

Wiggert D.C., Hatfield F.J. & Stuckenbruck S. 1987 *Analysis of liquid and structural transients by the method of characteristics*. ASME Journal of Fluids Engineering, Vol. 109, No. 2, pp. 161-165.

Wilkinson D.H. 1978 *Acoustic and mechanical vibrations in liquid-filled pipework systems*. Proc. BNES Int. Conf. on Vibration in Nuclear Plant, Keswick, UK, May 1978, Paper 8.5, pp. 863-878.

Wilkinson D.H. & Curtis E.M. 1980 *Water hammer in a thin-walled pipe*. Proc. of the 3rd Int. Conf. on Pressure Surges, BHRA, Canterbury, UK, March 1980, pp. 221-240.

Nomenclature

A	cross-sectional area
a	acceleration, deceleration
c	wave propagation speed
E	Young modulus of elasticity
F	force
f	friction coefficient
e	pipe wall thickness
g	gravitational acceleration
i_{OUT}	parameter regulating amount of numerical output
K	liquid bulk modulus
L	length
m	mass
N	normal force; number of pipe-dividing elements
P	pressure (cross-sectional average)
R	(inner) radius
s	sliding distance
t	time
u	axial displacement
$\dot{u}$	axial velocity
$\ddot{u}$	axial acceleration
V	fluid velocity (cross-sectional average)
z	axial coordinate
Δt	time step (numerical grid length on t-axis)
Δz	element length (numerical grid length on z-axis)
ε	axial strain
ν	Poisson ratio of pipe wall material
ρ	mass density
σ	axial stress
τ	rise time

Subscripts

C	Coulomb friction
f	fluid
r	rod
t	tube, pipe
0	constant value
1	one side of junction or pipe
2	other side of junction or pipe